Research Square

Preprints are preliminary reports that have not undergone peer review.
They should not be considered conclusive, used to inform clinical practice,
or referenced by the media as validated information.

Targeting BMI1 enhances cell adhesion to inhibit colorectal cancer progression and improve the efficacy of cetuximab

Yu Cheng
Wuhan University of Science and Technology
Hong-Shan Guo
Wuhan University of Science and Technology
Zhi-Wen Wang
Wuhan University of Science and Technology
Zhi Dai
Wuhan University of Science and Technology
Xiang Xiao
Wuhan University of Science and Technology
Wei Liu
Wuhan University of Science and Technology
Fei-Fei Qi
Wuhan University of Science and Technology
Ao Jiang
Wuhan University of Science and Technology
Ze Cai
Wuhan University of Science and Technology
Xing-Hua Liao
Wuhan University of Science and Technology
Jia-Peng Li
Wuhan University of Science and Technology
Jun Wang
wangjun0315@wust.edu.cn

Wuhan University of Science and Technology
Chao Lu
Tongji Hospital

Article

Keywords: Colorectal cancer, BMI1, Cell adhesion, MiR-218-5p, Resveratrol, Cetuximab

Posted Date: November 11th, 2026

DOI: https://doi.org/10.21203/rs.3.rs-11378574/v1

License: This work is licensed under a Creative Commons Attribution 4.0 International License.
Read Full License

Additional Declarations: No competing interests reported.

Targeting BMI1 enhances cell adhesion to inhibit colorectal cancer progression and improve the efficacy of cetuximab

Yu Cheng[1#], Hong-Shan Guo[1#], Zhi-Wen Wang[1, 2#], Zhi Dai[1], Xiang Xiao[1], Wei Liu[1], Fei-Fei Qi[1], Ao Jiang[1], Ze Cai[1], Xing-Hua Liao[1], Jia-Peng Li[1*], Jun Wang[1*], Chao Lu[3*]

1. Institute of Biology and Medicine, College of Life and Health Sciences, Wuhan University of Science and Technology, Wuhan, China.
2. Key Laboratory of Chronic Noncommunicable Diseases, Yueyang Vocational Technical College, Yueyang, Hunan, China.
3. Department of Thyroid and Breast Surgery, Tongji Hospital, Tongji Medical College, Huazhong University of Science and Technology, Wuhan, Hubei, China.

*Correspondence: Chao Lu, email: luchao817@163.com; Jun Wang, email: wangjun0315@wust.edu.cn; Jia-Peng Li, email: jiapengli@wust.edu.cn.

# These authors contributed equally to this work.

Abstract

Colorectal cancer (CRC) is a common malignant tumor with poor prognosis, urgently requiring new biomarkers and therapeutic targets. This study investigated the role of BMI1 in the progression of colorectal cancer and its regulatory mechanisms, as well as evaluated whether targeting BMI1 can enhance the efficacy of first-line drugs. BMI1 is highly expressed in colorectal cancer and promotes malignant progression by inhibiting cell adhesion. Knockdown of BMI1 suppresses its malignant behavior in both in vitro and in vivo experiments. MiR-218-5p targets the 3' UTR region of BMI1 and is downregulated in CRC; overexpression of miR-218-5p can reverse BMI1-mediated CRC progression. Furthermore, resveratrol targets and inhibits BMI1, thereby sensitizing CRC cells to the first-line EGFR-targeted drug cetuximab. The combination of resveratrol and cetuximab exhibits synergistic antitumor effects both in cultured cells and in vivo. In summary, this study elucidates the intervention role of miR-218-5p as an upstream regulator of BMI1 and confirms that resveratrol's targeted inhibition of BMI1 can enhance the therapeutic effect of cetuximab, providing new experimental evidence and strategies for molecular targeted combination therapy in colorectal cancer.

Keywords: Colorectal cancer, BMI1, Cell adhesion, MiR-218-5p, Resveratrol, Cetuximab.

Introduction

CRC is the third most common malignant tumor worldwide, with an increasing incidence among younger populations. It is estimated that the incidence will rise by 63% by 2040[1, 2] Surgery combined with radiotherapy and chemotherapy is the main treatment approach, but drug resistance is a significant issue, and the five-year survival rate for patients with metastasis is extremely low[3, 4]. Colonoscopy screening is limited by cost and patient compliance, resulting in limited effectiveness in prevention and control[5, 6]. Therefore, analyzing the abnormal expression and functional mechanisms of key genes is of great importance for identifying early biomarkers, elucidating the pathogenesis, and developing targeted therapies.

B-cell-specific Moloney murine leukemia virus integration site 1 (BMI1) gene was first discovered in lymphoma cells in 1991[7]. It is a core member of the Polycomb gene family and acts as an oncogene that can synergize with the proto-oncogene c-myc to drive cell transformation and tumor formation[8-10]. As a component of the Polycomb repressive complex 1 (PRC1), BMI1 is involved in chromatin epigenetic modification and the maintenance of stem cell homeostasis, functioning through the regulation of gene expression related to cell proliferation, apoptosis, DNA repair, and other processes[11, 12]. In malignant tumors such as breast cancer, oral squamous carcinoma, and gastric cancer, BMI1 can induce tumor cell migration and invasion[13-15]. Therefore, BMI1 is a potential target for CRC.

MiRNAs can act as oncogenic or tumor-suppressive factors in tumors such as gastric cancer, liver cancer, lung cancer, and breast cancer, regulating cell proliferation, apoptosis, angiogenesis, and metastasis[16-19]. Dysfunction may arise from genomic deletions, mutations, epigenetic modifications, or processing abnormalities, leading to dysregulation of target mRNA and protein expression[20]. Notably, tumor tissues often exhibit reduced expression of mature miRNAs[21]. As a tumor suppressor,

miR-218-5p targets CDK6 in gastric cancer to block the cell cycle and inhibit metastasis[22], in glioma, miR-218-5p targets CMTM3 to suppress cell proliferation and invasion[23], in breast cancer, it inhibits PINK1/Parkin-mediated mitophagy, enhancing sensitivity to doxorubicin[24]. Therefore, downregulation of miR-218-5p is a candidate driver gene in the development of multiple cancers.

This study focuses on the expression, function, mechanism, and clinical significance of BMI1 in CRC. We confirmed that BMI1 knockdown suppresses CRC cell proliferation, migration, and invasion by promoting cell adhesion; that miR-218-5p negatively regulates BMI1, and that resveratrol targets and inhibits BMI1 and can sensitize cells to cetuximab, thereby blocking the malignant progression of CRC.

Results

Elevated expression of BMI1 in CRC

To investigate the expression level of BMI1 in CRC, we examined BMI1 expression in CRC using the UALCAN and TCGA databases. The results showed that compared to adjacent normal tissues, BMI1 expression was elevated in CRC tumor tissues (Figures S1A-B). Further analysis using the UALCAN database revealed that BMI1 expression was associated with lymph node metastasis status and tumor staging in CRC patients (Figures S1C-D). To further analyze BMI1 expression in CRC, we collected tissue samples from 20 CRC patients. IHC staining analysis of BMI1 protein expression showed a significant increase in BMI1 levels in CRC tissues compared to adjacent normal tissues (Figure 1A). Subsequently, WB and RT-qPCR were used to detect BMI1 protein and mRNA expression levels in CRC tissues and their corresponding adjacent normal tissues. The results demonstrated that both protein and mRNA levels of BMI1 were elevated in CRC tissues compared to adjacent normal tissues (Figures 1B-1C). Similarly, compared to normal human colon epithelial cells (NCM460), BMI1 protein and mRNA expression levels were increased in CRC cell

lines SW480 and Caco-2 (Figures 1D-1E). The above results indicate that the expression level of BMI1 is upregulated in CRC and is associated with CRC progression.

Elevated BMI1 expression is associated with CRC cell proliferation migration and invasion

To investigate the functional role of BMI1 in the progression of CRC, we established stable BMI1 knockdown CRC cell lines. Among them, sh-BMI1-1 exhibited the highest knockdown efficiency and was used for subsequent functional validation (Figures 2A-D). CCK-8 assay results showed that knocking down BMI1 significantly reduced the viability of CRC cells (Figure S2A). EdU and colony formation assays further demonstrated that BMI1 knockdown inhibited the proliferative capacity of CRC cells (Figures S2B-2C). Additionally, wound healing and Transwell assays were performed to assess the effects of BMI1 on CRC cell migration and invasion. The wound healing assay indicated that BMI1 knockdown weakened the migratory ability of CRC cells (Figure 2E). The Transwell assay showed that BMI1 knockdown reduced the invasive capacity of CRC cells (Figure 2F). These results collectively suggest that BMI1 knockdown can inhibit the proliferation, migration, and invasion of CRC cells.

BMI1 promotes CRC progression by inhibiting cell adhesion

To elucidate the molecular mechanism by which BMI1 promotes CRC progression, we performed RNA-seq on SW480 cells from the sh-Control group and the sh-BMI1 group. The sequencing data were processed using the R package DESeq2, and the resulting differentially expressed genes were displayed in a volcano plot and heatmap. We found that 385 genes were upregulated and 468 genes were downregulated (Figures S3A-B). Next, we conducted biological process enrichment analysis on the differentially expressed genes, which showed that cell adhesion was significantly

enriched (Figure S3C). Tumor cells can enhance their proliferation, migration, and invasion abilities by inhibiting cell adhesion[25, 26]. The GO enrichment analysis also confirmed that BMI1 is associated with the cell adhesion process (Figures S3D-F). To validate our sequencing results, we performed Western blot experiments to detect the expression of cell adhesion-related proteins in CRC cells after BMI1 knockdown. The results showed that CDH1 expression was significantly increased, while EPCAM protein expression was significantly decreased after BMI1 knockdown (Figure 3A). Additionally, cell adhesion assays further confirmed that cell adhesion ability was enhanced following BMI1 knockdown (Figure 3B). These results indicate that BMI1 promotes CRC progression by inhibiting cell adhesion.

Knockdown of BMI1 inhibits malignant progression of CRC cells in vivo

Next, we investigated the effect of BMI1 on CRC in vivo using a nude mouse subcutaneous xenograft model. Caco-2 cells from the sh-BMI1 group and the sh-Control group were injected into the right axilla of 4-week-old male nude mice, with 6 replicates per group. The volume of the subcutaneous xenografts was measured every 7 days, and the mice were sacrificed after 28 days to collect the xenograft tumors. The results showed that, compared to the sh-Control group, the subcutaneous xenografts in the sh-BMI1 group grew more slowly and had relatively smaller volumes (Figures 4A-4B). Additionally, we weighed the subcutaneous xenograft tissues, and the results indicated that knockdown of BMI1 led to smaller tumor weights formed by the cells in the nude mice (Figure 4C). This suggests that knockdown of BMI1 can inhibit the tumorigenic ability of CRC cells in vivo. Furthermore, IHC staining analysis of the xenograft tissues revealed decreased expression levels of BMI1, Ki-67, EPCAM, and CDH2 in the sh-BMI1 group (Figure 4D). This further confirms that knockdown of BMI1 suppresses cell proliferation, migration, and invasion in vivo.

MiR-218-5p suppresses BMI1 expression by targeting its 3'UTR

To further identify miRNAs that can target BMI1, we predicted and intersected potential candidates using the miRDB, TarBase, and TargetScan databases, screening five potential miRNAs targeting the 3'UTR of BMI1 (miR-218-5p, miR-128-3p, miR-27a-3p, miR-27b-3p, and miR-203a-3p) (Figure 5A). Next, we examined the expression levels of these five miRNAs in normal human colon epithelial cells and CRC cells. The results showed that compared to normal human colon epithelial cells, the expression levels of miR-218-5p and miR-128-3p were significantly downregulated in CRC cells, whereas the expression levels of miR-27a-3p, miR-27b-3p, and miR-203a-3p were upregulated (Figure 5B). We then focused on the miR-218-5p and miR-128-3p, which were downregulated in CRC cells. Further dual-luciferase reporter assays demonstrated that miR-218-5p significantly inhibited the luciferase activity of the wild-type BMI1 3'UTR (WT-BMI1-3'UTR), but had no significant effect on the mutant BMI1 3'UTR (MUT-BMI1-3'UTR) (Figures 5C-D). Although miR-128-3p could suppress BMI1 transcriptional activity, its binding ability was relatively weak (Figures 5E-F). Therefore, in the subsequent experiments, we mainly focused on the regulatory effect of miR-218-5p on BMI1. Next, we further investigated whether miR-218-5p affects the protein expression level of BMI1. WB results showed that in SW480 and Caco-2 cells, overexpression of miR-218-5p significantly downregulated BMI1 protein levels, while inhibition of miR-218-5p significantly upregulated its expression (Figures S4A-4B). These results indicate that miR-218-5p can directly bind to the 3'UTR of BMI1, thereby suppressing its expression.

MiR-218-5p inhibits CRC cell proliferation, migration, and invasion by targeting BMI1

The expression levels of miR-218-5p in 20 pairs of CRC tissues and adjacent non-cancerous tissues were detected by RT-qPCR. The results showed that

miR-218-5p was significantly downregulated in CRC tissues (Figure S5A). Additionally, the expression level of miR-218-5p in the serum of CRC patients was also significantly lower compared to healthy individuals (Figure S5B). This indicates that miR-218-5p is lowly expressed in CRC and may be associated with the occurrence of CRC. Furthermore, we overexpressed miR-218-5p in CRC cells with or without BMI1 overexpression. The results showed that overexpression of miR-218-5p in CRC cells could inhibit the expression of BMI1 protein, while simultaneous overexpression of miR-218-5p and BMI1 rescued the inhibitory effect of miR-218-5p on BMI1 (Figures S5C-D). Next, we verified whether overexpression of miR-218-5p could restore the reduced adhesion ability of CRC cells mediated by BMI1. WB results showed that overexpression of BMI1 inhibited the expression level of CDH1 protein and increased the expression level of EPCAM protein, whereas simultaneous overexpression of BMI1 and miR-218-5p rescued the downregulation of CDH1 and upregulation of EPCAM protein expression caused by BMI1 overexpression (Figure 6A). The cell adhesion assay also confirmed that miR-218-5p can enhance the adhesion ability of CRC cells by targeting and inhibiting BMI1 (Figure 6B). In addition, the results of the CCK-8 assay, EdU assay, and colony formation assay showed that miR-218-5p can enhance the proliferation ability of CRC cells by targeting and inhibiting BMI1 (Figures S6A-C). The wound healing assay and Transwell assay results demonstrated that miR-218-5p can enhance the migration and invasion abilities of CRC cells by targeting and inhibiting BMI1 (Figures S7A-B). Next, we confirmed in vivo using a nude mouse subcutaneous tumor transplantation model that overexpression of BMI1 promotes tumor growth, while simultaneous overexpression of miR-218-5p can inhibit the tumor growth-promoting effect of BMI1 (Figures S8A-C). Additionally, we performed IHC staining analysis on tumor tissues, and the results showed that compared to the NC group, the expression levels of BMI1, Ki-67, EPCAM, and CDH2 were increased in the tumors of the BMI1 overexpression group. However, simultaneous overexpression of miR-218-5p

inhibited the BMI1-mediated upregulation of BMI1, Ki-67, EPCAM, and CDH2 expression (Figure S8D). This further demonstrates that miR-218-5p can enhance the adhesion ability of CRC cells by targeting and suppressing BMI1, thereby inhibiting the malignant progression of CRC.

Resveratrol targetedly inhibits BMI1 to enhance adhesion of CRC cells

Given the important role of BMI1 in the progression of CRC, conducting targeted drug research against BMI1 holds significant clinical value. We screened traditional Chinese medicine components that can target BMI1 through the HERB database, identifying diosgenin saponin and resveratrol. Among them, BMI1 shows a certain binding activity with resveratrol, whereas the binding activity between BMI1 and diosgenin saponin is very low (Figures 7A-B). Therefore, we selected resveratrol as the BMI1-targeting drug for subsequent studies. Next, we treated CRC cells with different concentrations of resveratrol to evaluate its inhibitory effect on cell viability. The results showed that resveratrol significantly inhibited the viability of CRC cells in a clear dose-dependent manner (Figure 7C). Further WB and RT-qPCR experiments demonstrated that resveratrol markedly suppressed both the protein and mRNA expression levels of BMI1 in CRC cells (Figures 7D-E). PTC-209 is a specific BMI1 inhibitor. We next compared the cytotoxicity of the two drugs. The results showed that, compared to PTC-209, resveratrol exhibited lower toxicity to human normal colon epithelial (NCM-460 cells) (Figure 7F). These results indicate that resveratrol can inhibit the expression of BMI1 and, given its lower toxicity to normal cells, is more suitable as a potential targeted drug for BMI1.

Resveratrol inhibits CRC progression by enhancing cell adhesion

We further evaluated the effect of resveratrol on the adhesion ability of CRC cells. WB analysis showed that compared to the DMSO group, resveratrol treatment increased the expression level of CDH1 and decreased the expression level of

EPCAM (Figure 8A). Cell adhesion assays also confirmed that resveratrol treatment enhanced cell adhesion ability (Figure 8B). Furthermore, CCK-8, EdU, and colony formation assays demonstrated that resveratrol treatment inhibited the proliferation of CRC cells (Figures S9A-B). Wound healing and transwell assays showed that resveratrol treatment suppressed the migration and invasion of CRC cells (Figures S9C-D). Subsequently, using a nude mouse subcutaneous xenograft model, we confirmed in vivo that resveratrol could inhibit tumor growth in mice (Figures 8C-E). Further IHC results indicated that the expression levels of BMI1, Ki-67, EPCAM, and CDH2 were relatively lower in tumor tissues from the resveratrol treatment group (Figure 8F). These results suggest that resveratrol can inhibit the malignant progression of CRC.

Resveratrol synergizes with cetuximab to inhibit CRC progression

Cetuximab is a first-line treatment for CRC with wild-type RAS/BRAF genes, but some patients develop resistance. Studies have shown that dysregulation of cell adhesion-related proteins leads to reduced efficacy of cetuximab in CRC[27]. Therefore, we investigated whether resveratrol could enhance the adhesion ability of cells treated with cetuximab. Caco-2 cells are a RAS/BRAF wild-type cell line, while SW480 cells are a RAS mutant cell line. The results showed that, compared to the single-drug groups, the adhesion ability of cells in the combination treatment group was significantly enhanced in both Caco-2 and SW480 cells (Figures 9A-B). Furthermore, compared to the single-drug groups, the combination treatment not only inhibited proliferation, migration, and invasion abilities of Caco-2 cells but also significantly suppressed proliferation, migration, and invasion of SW480 cells (Figures S10A-D). Additionally, using a nude mouse subcutaneous xenograft model, we confirmed in vivo that resveratrol and cetuximab synergistically inhibited tumor growth in mice (Figures 9C-E). IHC results showed that, compared to the single-drug groups, the expression levels of BMI1, Ki-67, EPCAM, and CDH2 in tumor tissues

were significantly reduced in the combination treatment group (Figure 9F). These results indicate that resveratrol can synergize with cetuximab to inhibit malignant progression of CRC.

Discussion

BMI1 is highly expressed and plays an oncogenic role in various tumors, in breast cancer, it regulates the cell cycle, proliferation, and apoptosis processes to promote malignant progression[28], in neuroblastoma, the BMI1 inhibitor PTC-028 can activate the p53 pathway, downregulate anti-apoptotic proteins, and induce apoptosis and cell cycle arrest[29], in acute myeloid leukemia, high BMI1 expression is associated with poor prognosis, and its inhibitor PTC-209 can target leukemia stem cells and induce apoptosis[30]. This study confirmed that BMI1 is highly expressed in colorectal cancer tissues and CRC cell lines, and knocking down BMI1 significantly inhibited CRC progression. Further analysis revealed that BMI1 exerts its tumor-promoting effect by suppressing cell adhesion, while miR-218-5p can inhibit this effect by targeting the 3'UTR of BMI1 to suppress its expression. In addition, inhibition of BMI1 enhanced the sensitivity of CRC to cetuximab (Figures S11).

MiR-218-5p acts as a suppressor in various tumors, and its downregulation is involved in tumor progression[24, 31]. This study confirmed that miR-218-5p is significantly underexpressed in CRC cells, tissues, and serum samples. Studies have demonstrated that miR-218-5p influences the progression of multiple tumors through various regulatory pathways. miR-218-5p can simultaneously inhibit SNAI2 and FTH1P3, forming a positive feedback loop among the three, thereby suppressing CRC metastasis[32]. The lncRNA TINCR can act as a competitive endogenous RNA (ceRNA) sponge to absorb miR-218-5p, thereby upregulating the expression of DDX5 and indirectly promoting the proliferation and migration of liver cancer cells, which indirectly confirms the inhibitory role of miR-218-5p[33]. In retinoblastoma,

miR-218-5p suppresses cell growth by targeting NACC1 and inhibiting the AKT/mTOR signaling pathway[34]. This study further found that miR-218-5p can directly target and negatively regulate BMI1, restoring miR-218-5p to target BMI1 effectively inhibits CRC cell proliferation, migration, and invasion.

Resveratrol is a natural polyphenolic compound with anti-inflammatory, antioxidant, and broad-spectrum antitumor activities. It can regulate multiple pathways to exert antitumor effects[35-38], reverse EMT, and sensitize chemoresistance[39, 40]. Compared to the BMI1 inhibitor PTC-209, it exhibits lower toxicity to normal colon cells and better safety. Previous studies have confirmed that resveratrol can inhibit colorectal cancer proliferation and metastasis through multiple signaling pathways. This study found that it can upregulate CDH1 and downregulate EPCAM, enhancing the adhesion ability of CRC cells, while inhibiting cell proliferation, migration, and invasion. At the same time, it clarified a new mechanism by which BMI1 inhibition can enhance cell adhesion. Cetuximab resistance greatly limits its application in RAS/BRAF wild-type metastatic CRC, and the combined use of natural active substances is an important strategy to reverse resistance. Previous studies have confirmed that platycodin D and honokiol can both enhance the sensitivity of CRC cells to cetuximab[41, 42]. This study found that cetuximab alone has a weak regulatory effect on CRC cell adhesion, but when combined with resveratrol, it can upregulate CDH1 and downregulate EPCAM, thereby enhancing cell adhesion and significantly improving the antitumor effect. Thus producing a synergistic antitumor effect with cetuximab.

In summary, this study confirms that BMI1 is highly expressed in CRC and promotes tumor proliferation, migration, and invasion by inhibiting cell adhesion. MiR-218-5p is found at low levels in the tissues and serum of CRC patients and can negatively regulate BMI1 expression by targeting its 3'UTR. Furthermore, the natural compound

resveratrol was found to directly target and inhibit BMI1, enhance cell adhesion ability, and significantly increase the sensitivity of CRC to cetuximab treatment. Our research reveals a new mechanism by which BMI1 promotes CRC progression through the inhibition of cell adhesion and provides insights for the clinical diagnosis and treatment of CRC.

Materials and Methods

Cell Lines

NCM460, SW480, Caco-2, and HEK-293T cell lines were obtained from Procell. The three cell lines, SW480, Caco-2, and HEK-293T, were cultured in high-glucose DMEM complete medium, while the NCM460 cell line was cultured in RPMI 1640 complete medium. All media were supplemented with 10% fetal bovine serum and 1% penicillin-streptomycin (100×). All cells were incubated at 37 ℃ in an atmosphere containing 5% CO_2.

Patients and Tissue Samples

The CRC patient samples (including the patient's peritumoral tissue, tumor tissue, and serum) used in this study were all obtained from Tongji Hospital, Tongji Medical College, Huazhong University of Science and Technology, collected from December 2022 to January 2025. All CRC patients met the diagnostic criteria for colorectal cancer. In addition, we also collected serum samples from 15 healthy volunteers. All experiments involving human specimens have been reviewed and approved by the Medical Ethics Committee of Huazhong University of Science and Technology, and strictly adhere to the ethical guidelines required and advocated by the Declaration of Helsinki. All patients participating in this study signed informed consent forms.

CCK-8 Assay

Seed cells into a 96-well plate at the preset cell density (three replicates per well,

including blank controls and zeroing wells). After culturing in the incubator until the cells adhere, treat the cells with drugs according to the grouping. At the preset time point, directly add 10% CCK-8 reagent to each well, incubate at 37°C in the dark for 30 minutes, then measure the absorbance at 450 nm using a microplate reader and calculate the relative cell viability.

Colony Formation Assay

In the colony formation analysis, cells were seeded at low density into 6-well plates and cultured for 14 days. During this period, the formation of cell colonies was regularly observed, and fresh culture medium was replaced. After colony formation, cells were fixed with methanol and stained with 0.1% crystal violet. The number of cell colonies was quantified using ImageJ software.

Wound Healing Assay

To evaluate cell migration, a confluent monolayer of cells in 6-well plates was scratched with the tip of a sterile pipette to create a wound. Detached cells were removed by washing with PBS. The process of cell migration into the wound area was monitored at 0 h and 36 h using a microscope. The scratch area was quantified using ImageJ software.

Transwell Assay

Cell migration was assessed using Transwell chambers (8.0 μm pore size). Cells were seeded into the upper chamber with serum-free medium, while the lower chamber contained medium supplemented with 20% FBS as a chemoattractant. After 48 h, cells that had migrated or invaded through the membrane were fixed with methanol and stained with 0.1% crystal violet. The number of cells was quantified under a microscope.

5-Ethynyl-2′-deoxyuridine （EdU） cell proliferation assay

Log-phase cells at 2×10^5 cells per well were seeded into 12-well plates. After 24 h of culture, 10 μM EdU working solution was added, and the cells were incubated at 37 ℃ in the dark for 2 h. Cells were fixed with 4% paraformaldehyde at room temperature for 30 min, permeabilized with 0.1% Triton X-100 at room temperature for 10 min, then incubated with Click reaction solution in the dark for 30 min. Cell nuclei were counterstained with DAPI. After washing with PBS, cells were observed and photographed under an inverted fluorescence microscope, and the proportion of EdU-positive cells was calculated.

Cell Adhesion

A 96-well plate was coated with fibronectin at 10 μg/mL at room temperature for 24 h, then washed with serum-free medium. Log-phase cells were seeded at 5×10^3 cells per well onto the coated plate and incubated at 37 °C for 6 h, followed by gentle washing with PBS. The cells were then fixed, stained, and observed under an inverted microscope for photography and counting of adherent cells.

Immunohistochemical Staining

Paraffin sections were dewaxed and rehydrated through a graded ethanol series, antigen retrieval was performed using sodium citrate. Incubation with 3% H_2O_2 was carried out in the dark for 15 min, blocking was done with 3% BSA for 30 min. Primary antibody incubation was performed overnight at 4 °C, followed by secondary antibody incubation at room temperature for 1 h. DAB was used for color development, followed by hematoxylin counterstaining, differentiation, and bluing, dehydration, clearing, and mounting were then performed. Microscopic observation and semi-quantitative analysis using the H-score method were conducted.

Western Blot (WB)

Prepare the electrophoresis gel using the gel preparation kit. Load equal amounts of protein samples and run the electrophoresis until the bromophenol blue dye reaches the bottom of the gel. Perform wet transfer. Block the PVDF membrane with 5% skim milk at room temperature for 2 h, then incubate overnight at 4 °C with primary antibodies (anti-BMI1, anti-CDH1, anti-EPCAM) diluted in 3% BSA. Wash the membrane with TBST, incubate with HRP-conjugated secondary antibody at room temperature for 1 h, and wash again with TBST. Develop the membrane using ECL chemiluminescent substrate and perform quantitative analysis of the grayscale values. The following antibodies were used: anti-BMI1 (1:1000, 66161-1-Ig, proteintech, Wuhan, China), anti-CDH1 (1:1000, A20798, ABclone, Wuhan, China), anti-EPCAM (1:1000, 21050-1-AP, proteintech, Wuhan, China), β-actin (1:5000, AC028, ABclone, Wuhan, China).

RT-qPCR Analysis

Total RNA was extracted using an ultrapure RNA kit according to the manufacturer's instructions. Subsequently, the total RNA was reverse transcribed into complementary DNA (cDNA) using the ABScript II cDNA First Strand Synthesis Kit. Primer sequences are listed in Supplemental Table 1. β-actin was selected as the housekeeping gene to normalize the data for each target gene.

Construction of Mouse Tumor Model

This experiment was approved by the Animal Ethics Committee of Wuhan University of Science and Technology. Four-week-old male BALB/c nude mice (purchased from Wuhan Shubeili Biotechnology Co., Ltd., with similar body weights) were subcutaneously inoculated with 1×10^7 cells per mouse. Starting from day 7 after inoculation, tumor volume was measured daily. When the tumor volume reached 100-150 mm^3, treatment began: resveratrol (50 mg/kg, intraperitoneal injection, every

other day), cetuximab (1 mg per mouse, intraperitoneal injection, twice weekly), and a combination group receiving both drugs. The control group was given an equal volume of DMSO. Tumor growth curves were plotted using the formula V = length × width² × 1/2. On day 28, mice were euthanized by gradual CO_2 inhalation (30%-70% chamber volume per minute) combined with cervical dislocation. Tumors were excised and weighed; some were fixed in 4% paraformaldehyde, while others were snap-frozen in liquid nitrogen and stored at -80 °C.

Transcriptome Sequencing

Total RNA was extracted from each group of tumor cells for transcriptome sequencing. Gene ontology enrichment analysis and pathway enrichment analysis were performed on the sequencing data using R packages. Genes with an adjusted $p < 0.05$ were identified as significantly differentially expressed between groups and were selected for subsequent functional validation according to experimental requirements.

Bioinformatics Analysis

The expression and clinical relevance of BMI1 in colorectal cancer were analyzed using the UALCAN (http://ualcan.path.uab.edu) and TCGA (https://portal.gdc.cancer.gov/) databases. MiRNAs targeting the 3'UTR of BMI1 were predicted using miRDB (https://mirdb.org/), TargetScan (http://www.targetscan.org/vert_72/), and TarBase (https://dianalab.e-ce.uth.gr). Molecular docking was employed to investigate drug-target interactions, BMI1-targeting compounds were screened from the HERB database, and the three-dimensional structures of BMI1 and small molecules were obtained. Semi-flexible docking was performed using AutoDockTools-1.5.7 to calculate binding energies, and docking results were visualized with PyMOL 2.6.0.

Statistical Analysis

In this chapter, GraphPad Prism software was used for statistical analysis of the experimental results. The experimental results are derived from three independent experiments. Data in this chapter are presented as Mean ± SD. The significance between two groups of experimental data was analyzed using the Student's *t*-test. For comparisons among multiple groups, one-way ANOVA was used when there was only one grouping variable, two-way ANOVA was used when there were two grouping variables. In the figures, * indicates $p < 0.05$, ** indicates $p < 0.01$, *** indicates $p < 0.001$, and *NS* indicates no statistical significance.

Data availability statement

RNA-Seq data were deposited into the Gene Expression Omnibus database under accession number GSE351220 and are available at the following URL: https://www.ncbi.nlm.nih.gov/geo/query/acc.cgi?acc=GSE351220.

Acknowledgments

Not applicable.

Funding

This work was financially supported by the National Natural Science Foundation of China (82203497, 82605121). Hubei Provincial Natural Science Foundation of China (2025AFB122, 2025AFD005 and 2024AFB905), Department of Education Scientific Research Program guidance project (B2023014), “The 14th Five Year Plan” Hubei Provincial advantaged characteristic disciplines (gropus) project of Wuhan University of Science and Technology (2023C0303), Natural Science Foundation Exploration Program of Wuhan (2024040801020310), StateKeyLaboratory of Neurology and Oncology Drug Development (2024040801020310).

Ethics approval and consent to participate

All human specimen (including CRC patients and healthy volunteers) in this study were approved and reviewed by the Medical Ethics Committee of Huazhong University of Science and Technology, obtained with the consent of the subjects, and conducted in accordance with the Declaration of Helsinki. All animal experiments were performed in compliance with the ARRIVE guidelines. The study was approved by the Ethics Committee of Wuhan University of Science and Technology. All methods were carried out in accordance with the relevant guidelines and regulations.

CRediT authorship contribution statement

Conceptualization: J.P.L., J.W. and C.L. Experiment lead: Y.C., H.S.G. and J.W. Analytic lead: Z.W.W., X.X., W.L. and F.F. Q. Assistance: Z.D., A.J. and Z.C. Manuscript prep: Y.C. and H.S.G. Supervision: J.W. and C.L. Research funding: X.H.L., J.P.L. and J.W. All authors reviewed the manuscript.

Declaration of competing interest

The authors declare no competing interests.

References

[1] Sung H, Ferlay J, Siegel RL, Laversanne M, Soerjomataram I, Jemal A, Bray F (2021). Global Cancer Statistics 2020: GLOBOCAN Estimates of Incidence and Mortality Worldwide for 36 Cancers in 185 Countries *CA Cancer J Clin* **71**, 209-249.

[2] Zhang T, Guo Y, Qiu B, Dai X, Wang Y, Cao X (2024). Global, regional, and national trends in colorectal cancer burden from 1990 to 2021 and projections to 2040 *Front Oncol* **14**, 1466159.

[3] Steup C, Kennel KB, Neurath MF, Fichtner-Feigl S, Greten FR (2025). Current and emerging concepts for systemic treatment of metastatic colorectal cancer *Gut* **74**, 2070-2095.

[4] Biller LH, Schrag D (2021). Diagnosis and Treatment of Metastatic Colorectal Cancer: A Review *Jama* **325**, 669-685.

[5] Li J, Pan J, Wang L, Ji G, Dang Y (2025). Colorectal Cancer: Pathogenesis and Targeted Therapy *MedComm (2020)* **6**, e70127.

[6] Ramos MC, Passone JAL, Lopes ACF, Safatle-Ribeiro AV, Ribeiro Júnior U, de Soárez PC (2023). Economic evaluations of colorectal cancer screening: A systematic review and quality assessment *Clinics (Sao Paulo)* **78**, 100203.

[7] Haupt Y, Alexander WS, Barri G, Klinken SP, Adams JM (1991). Novel zinc finger gene implicated as myc collaborator by retrovirally accelerated lymphomagenesis in E mu-myc transgenic mice *Cell* **65**, 753-763.

[8] Qin Z, Liu S, Zheng Y, Wang Y, Chen Y, Peng X, Jia L (2025). Co-targeting BMI1 and MYC to eliminate cancer stem cells in squamous cell carcinoma *Cell Rep Med* **6**, 102077.

[9] Jacobs JJ, Scheijen B, Voncken JW, Kieboom K, Berns A, van Lohuizen M (1999). Bmi-1 collaborates with c-Myc in tumorigenesis by inhibiting c-Myc-induced apoptosis via INK4a/ARF *Genes Dev* **13**, 2678-2690.

[10] Haupt Y, Bath ML, Harris AW, Adams JM (1993). bmi-1 transgene induces lymphomas and collaborates with myc in tumorigenesis *Oncogene* **8**, 3161-3164.

[11] Chen Y, Liu S, Yin X (2025). Progress and prospects of the combination of BMI1-targeted therapy and immunotherapy in cervical cancer *Am J Cancer Res* **15**, 217-232.

[12] Jung Y, Nolta JA (2016). BMI1 Regulation of Self-Renewal and Multipotency in Human Mesenchymal Stem Cells *Curr Stem Cell Res Ther* **11**, 131-140.

[13] Chen D, Wu M, Li Y, Chang I, Yuan Q, Ekimyan-Salvo M, Deng P, Yu B, Yu Y, Dong J, et al. (2017). Targeting BMI1(+) Cancer Stem Cells Overcomes Chemoresistance and Inhibits Metastases in Squamous Cell Carcinoma *Cell Stem Cell* **20**, 621-634.e626.

[14] Guo BH, Feng Y, Zhang R, Xu LH, Li MZ, Kung HF, Song LB, Zeng MS (2011). Bmi-1 promotes invasion and metastasis, and its elevated expression is correlated with an advanced stage of breast cancer *Mol Cancer* **10**, 10.

[15] Li Y, Tian Z, Tan Y, Lian G, Chen S, Chen S, Li J, Li X, Huang K, Chen Y (2020). Bmi-1-induced miR-27a and miR-155 promote tumor metastasis and chemoresistance by targeting RKIP in gastric cancer *Mol Cancer* **19**, 109.

[16] Yu X, Zhang Y, Luo F, Zhou Q, Zhu L (2024). The role of microRNAs in the gastric cancer tumor microenvironment *Mol Cancer* **23**, 170.

[17] Song G, Yu X, Shi H, Sun B, Amateau S (2024). miRNAs in HCC, pathogenesis, and targets *Hepatology*.

[18] Shrestha C, Brito S, Deshar B, Cho J, Lee G, Jung D, Park J, Min KS, Chae YK, Kim J (2026). MicroRNA-regulated signaling and tumor microenvironment modulation in lung cancer: mechanistic insights and translational opportunities *Cancer Cell Int* **26**.

[19] Ismail A, El-Mahdy HA, Abulsoud AI, Sallam AM, Eldeib MG, Elsakka EGE, Zaki MB, Doghish AS (2023). Beneficial and detrimental aspects of miRNAs as chief players in breast cancer: A comprehensive review *Int J Biol Macromol* **224**, 1541-1565.

[20] Choudhary A, Kumar A, Munshi A (2025). Genetic variants in oncogenic miRNA and 3' untranslated region of tumor suppressor genes: emerging insight into cancer genetics *Med Oncol* **42**, 303.

[21] Meng F, Zhang M, Pu D, Shi G, Li J (2025). Dual-regulatory miRNAs: master regulators and therapeutic targets in bone-metastatic breast cancer *Front Mol Biosci* **12**, 1680908.

[22] Deng M, Zeng C, Lu X, He X, Zhang R, Qiu Q, Zheng G, Jia X, Liu H, He Z (2017). miR-218 suppresses gastric cancer cell cycle progression through the CDK6/Cyclin D1/E2F1 axis in a feedback loop *Cancer Lett* **403**, 175-185.

[23] Li X, Lu T, Wang T, Zhuo J, Yu Z, Cui G, Shen H (2026). MiR-218-5p inhibits glioma progression by targeting CKLF-like MARVEL transmembrane domain-containing 3 *BMC Cancer* **26**, 234.

[24] Naso FD, Bruqi K, Manzini V, Chiurchiù V, D'Onofrio M, Arisi I, Strappazzon F (2024). miR-218-5p and doxorubicin combination enhances anticancer activity in breast cancer cells through Parkin-dependent mitophagy inhibition *Cell Death Discov* **10**, 149.

[25] Fares J, Fares MY, Khachfe HH, Salhab HA, Fares Y (2020). Molecular principles of metastasis: a hallmark of cancer revisited *Signal Transduct Target Ther* **5**, 28.

[26] Kou Y, Zhu R, Gu F, Tang H, Yang R, Wang Y, Wang Y, Han B (2026). Dioscin suppresses epithelial-mesenchymal transition in gastric cancer by upregulating Cx43 to inhibit the VEGFA/PI3K/Akt/mTOR pathway *Phytomedicine* **150**, 157646.

[27] Zhang X, Zhou W, Wu C, Jiang J, Guo Q, Feng L, Cheng X, Zhang X (2024). Cetuximab inhibits colorectal cancer development through inactivating the Wnt/β-catenin pathway and modulating PLCB3 expression *Sci Rep* **14**, 10642.

[28] Szustka A, Krześlak A (2024). BMI-1 in Breast Cancer - Biological Role and Clinical Implications *Cell Physiol Biochem* **58**, 584-596.

[29] Hirayama M, Yamada E, Aoki H, Izumi K, Amano A, Toriuchi K, Ogami K, Nagasaka M, Inoue Y, Hayashi H, et al. (2025). Pharmacologic inhibition of BMI1 exerts antitumor effects against MYCN-amplified neuroblastoma, with activation of the p53 pathway *Sci Rep* **15**, 22917.

[30] Nishida Y, Maeda A, Chachad D, Ishizawa J, Qiu YH, Kornblau SM, Kimura S, Andreeff M, Kojima K (2015). Preclinical activity of the novel B-cell-specific Moloney murine leukemia virus integration site 1 inhibitor PTC-209 in acute myeloid leukemia: Implications for leukemia therapy *Cancer Sci* **106**, 1705-1713.

[31] Zhu K, Ding H, Wang W, Liao Z, Fu Z, Hong Y, Zhou Y, Zhang CY, Chen X (2016). Tumor-suppressive miR-218-5p inhibits cancer cell proliferation and migration via EGFR in non-small cell lung cancer *Oncotarget* **7**, 28075-28085.

[32] Deng H, Zhang Q, Zhao Z, Wang M, Xu Q (2024). SNAI2/FTH1P3/miR-218-5p Positive Feedback Loop Promotes Colorectal Cancer Metastasis *Biochem Genet* **62**, 2210-2223.

[33] Zhao H, Xie Z, Tang G, Wei S, Chen G (2020). Knockdown of terminal differentiation induced ncRNA (TINCR) suppresses proliferation and invasion in hepatocellular carcinoma by targeting the miR-218-5p/DEAD-box helicase 5 (DDX5) axis *J Cell Physiol* **235**, 6990-7002.

[34] Li L, Yu H, Ren Q (2020). MiR-218-5p Suppresses the Progression of Retinoblastoma Through Targeting NACC1 and Inhibiting the AKT/mTOR Signaling Pathway *Cancer Manag Res* **12**, 6959-6967.

[35] Arif M, Pandey P, Khan F (2024). Review Deciphering the Anticancer Efficacy of Resveratrol and their Associated Mechanisms in Human Carcinoma *Endocr Metab Immune Disord Drug Targets* **24**, 1015-1026.

[36] Talib WH, Al Junaidi HS, Hadi RW, Ashour TH, Zabout IZ, Sabri SM, Alshaeri HK, Law D, Hock M, Prémusz V (2026). Targeting cancer hallmarks using resveratrol: isolation, formulation, and mechanisms of action *Front Nutr* **13**, 1747820.

[37] Ahmadi R, Ebrahimzadeh MA (2020). Resveratrol - A comprehensive review of recent advances in anticancer drug design and development *Eur J Med Chem* **200**, 112356.

[38] Varoni EM, Lo Faro AF, Sharifi-Rad J, Iriti M (2016). Anticancer Molecular Mechanisms of Resveratrol *Front Nutr* **3**, 8.

[39] Bhuia MS, Chowdhury R, Akter MA, Ali MA, Afroz M, Akbor MS, Sonia FA, Mubarak MS, Islam MT (2024). A mechanistic insight into the anticancer potentials of resveratrol: Current perspectives *Phytother Res* **38**, 3877-3898.

[40] Xu J, Liu D, Niu H, Zhu G, Xu Y, Ye D, Li J, Zhang Q (2023). Correction: Resveratrol reverses Doxorubicin resistance by inhibiting epithelial-mesenchymal transition (EMT) through modulating PTEN/ Akt signaling pathway in gastric cancer *J Exp Clin Cancer Res* **42**, 23.

[41] Liu Y, Tian S, Yi B, Feng Z, Chu T, Liu J, Zhang C, Zhang S, Wang Y (2022). Platycodin D sensitizes KRAS-mutant colorectal cancer cells to cetuximab by inhibiting the PI3K/Akt signaling pathway *Front Oncol* **12**, 1046143.

[42] Zhu Q, Zhang R, Gu X, Zhao Z, Gao Q, Chen M, Wu Q, Xie T, Sui X (2024). Honokiol enhances the sensitivity of cetuximab in KRAS(G13D) mutant colorectal cancer through destroying SNX3-retromer complex *Theranostics* **14**, 5443-5460.

Figure legends

Figure. 1 BMI1 expression is elevated in CRC.

A. Representative images and scoring statistics of BMI1 IHC in CRC tumor tissues and their paired adjacent non-cancerous tissues. Scale bar:50 μm. B. Representative WB bands showing BMI1 expression in paired tissues from 8 CRC patients and the corresponding band intensity quantification results. C. Relative mRNA expression levels of BMI1 in 20 CRC tissue samples detected by RT-qPCR. D. WB detection of BMI1 expression in CRC cell lines and normal colonic epithelial cells NCM460, along with quantitative statistical charts. E. RT-qPCR detection of differences in BMI1 gene expression in SW480, Caco-2, and NCM460 cells. * represents $p< 0.05$, ** represents $p< 0.01$, *** represents $p< 0.001$.

Figure. 2 Elevated BMI1 expression is associated with CRC cell proliferation migration and invasion.

A. WB assay was used to detect the protein expression levels of BMI1 in SW480 cells in the sh-Control, sh-BMI1-1, sh-BMI1-2, and sh-BMI1-3 groups. The WB signal was quantified and normalized to β-actin, and the results were presented as a histogram. B. RT-qPCR detection of BMI1 mRNA expression levels in various treatment groups of SW480 cells. C. WB assay was used to detect the protein expression levels of BMI1 in Caco-2 cells in the sh-Control, sh-BMI1-1, sh-BMI1-2, and sh-BMI1-3 groups. The WB signal was quantified and normalized to β-actin, and the results were presented as a histogram. D. RT-qPCR detection of BMI1 mRNA expression levels in various treatment groups of Caco-2 cells. E. Cell wound healing assay to detect the effect of BMI1 knockdown on the migration ability of CRC cells and quantitative analysis of the wound healing rate. Scale bar: 100 μm. F. Transwell assay to evaluate the effect of BMI1 knockdown on the invasive ability of CRC cells and quantitative analysis results. Scale bar: 100 μm. * represents $p< 0.05$, ** represents $p< 0.01$, *** represents $p< 0.001$.

Figure. 3 BMI1 promotes CRC progression by inhibiting cell adhesion.

A. WB assay was used to detect the expression levels of cell adhesion-related proteins in CRC cells of the sh-Control and sh-BMI1 groups. The WB signal was quantified and normalized to β-actin, and the results were presented as a histogram. B. Cell adhesion assay was used to evaluate the effect of BMI-1 knockdown on the adhesion ability of CRC cells, and the results of the cell adhesion assay were quantitatively analysed. Scale bar: 100 μm. * represents $p< 0.05$, ** represents $p< 0.01$, *** represents $p< 0.001$.

Figure. 4 Knockdown of BMI1 inhibits the malignant progression of CRC cells in vivo.

A. Typical images of nude mouse subcutaneous xenografts. B. Tumor growth curves of nude mice in each group. C. Tumor weight statistics of nude mice in each group. D. IHC analysis of the expression levels of BMI1, Ki-67, EPCAM, and CDH2 in nude mouse subcutaneous xenograft tissues. Scale bar: 100 μm. ** represents $p < 0.01$.

Figure. 5 MiR-218-5p inhibits the expression of BMI1 by targeting its 3'UTR.

A. Prediction of miRNAs that could bind to the 3'UTR of BMI1 using miRDB, TargetScan, and TarBase databases, followed by intersection analysis presented in a Venn diagram. B. RT-qPCR detection of the expression levels of miR-218-5p, miR-128-3p, miR-27a-3p, miR-27b-3p, and miR-203a-3p in human normal colonic epithelial cells and CRC cells. C. Schematic diagram of the luciferase reporter plasmid containing the binding site and mutant site of miR-218-5p with the 3'UTR sequence of BMI1. D. Dual-luciferase reporter assay validating the binding of miR-218-5p to the BMI1 3'UTR. E. Schematic diagram of the luciferase reporter plasmid containing the binding site and mutant site of miR-128-3p with the 3'UTR sequence of BMI1. F. Dual-luciferase reporter assay validating the binding of

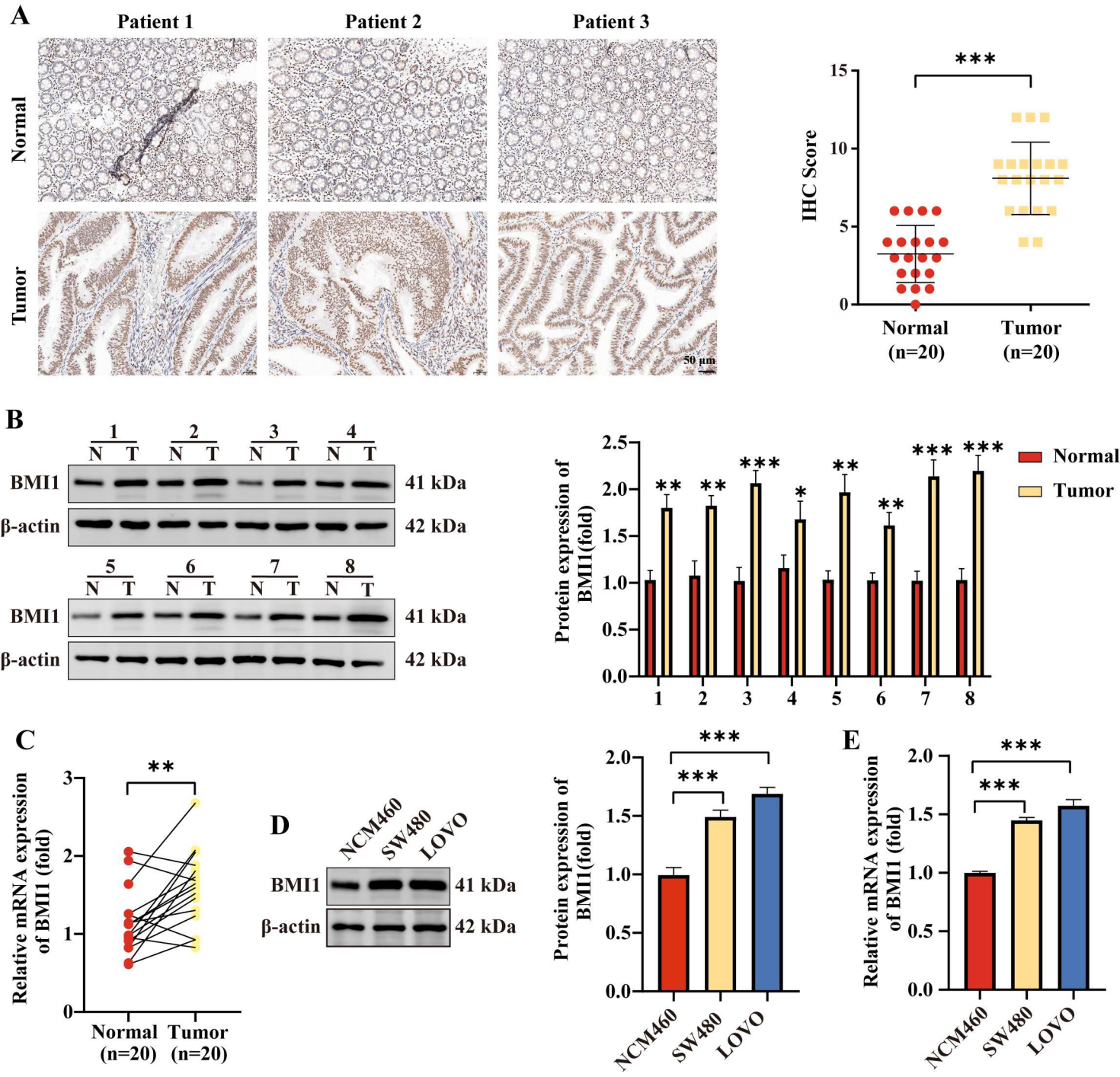
677 miR-216a-5p to the BMI1 3'UTR. * represents $p< 0.05$, ** represents $p< 0.01$, ***
678 represents $p< 0.001$, *NS* represents no statistical significance.
679
680 **Figure. 6 MiR-218-5p inhibits the proliferation, migration, and invasion of CRC**
681 **cells by targeting BMI1.**
682 A. Overexpress miR-218-5p in SW480 cells with or without BMI1 overexpression,
683 and detect the expression levels of cell adhesion-related proteins in the cells by WB,
684 quantify the WB signals normalized to β-actin, and present the results as histograms.
685 B. Overexpressing miR-218-5p in CRC cells with or without BMI1 overexpression,
686 cell adhesion assays were used to evaluate the adhesion ability of SW480 cells, and
687 the results of the cell adhesion assays were quantitatively analysed.** represents $p<$
688 0.01, *** represents $p< 0.001$.
689
690 **Figure. 7 Resveratrol targets and inhibits BMI1 to enhance adhesion of CRC**
691 **cells.**
692 A. Drugs targeting BMI1 based on analysis from various databases, as well as the
693 biological binding sites and binding energies of each drug with BMI1. B. Molecular
694 docking of diosgenin saponins, resveratrol, and BMI1. C. Determination of the
695 proliferation activity of CRC cells treated with gradient concentrations of resveratrol
696 using the CCK-8 assay method. D. Treat CRC cells with resveratrol (60 μM) for 48 h,
697 then use WB to detect the protein expression level of BMI1 in the cells, quantify the
698 WB signals normalized to β-actin and present the results as a histogram. E. CRC cells
699 were treated with resveratrol (60 μM) for 48 h, and the mRNA expression levels of
700 BMI1 were detected by RT-qPCR. F. Human normal colonic epithelial cells were
701 treated with resveratrol (60 μM) or PTC-209 (10 μM) for 48 h, and cell viability was
702 assessed by CCK-8 assay. ** represents $p< 0.01$, *** represents $p< 0.001$.
703
704

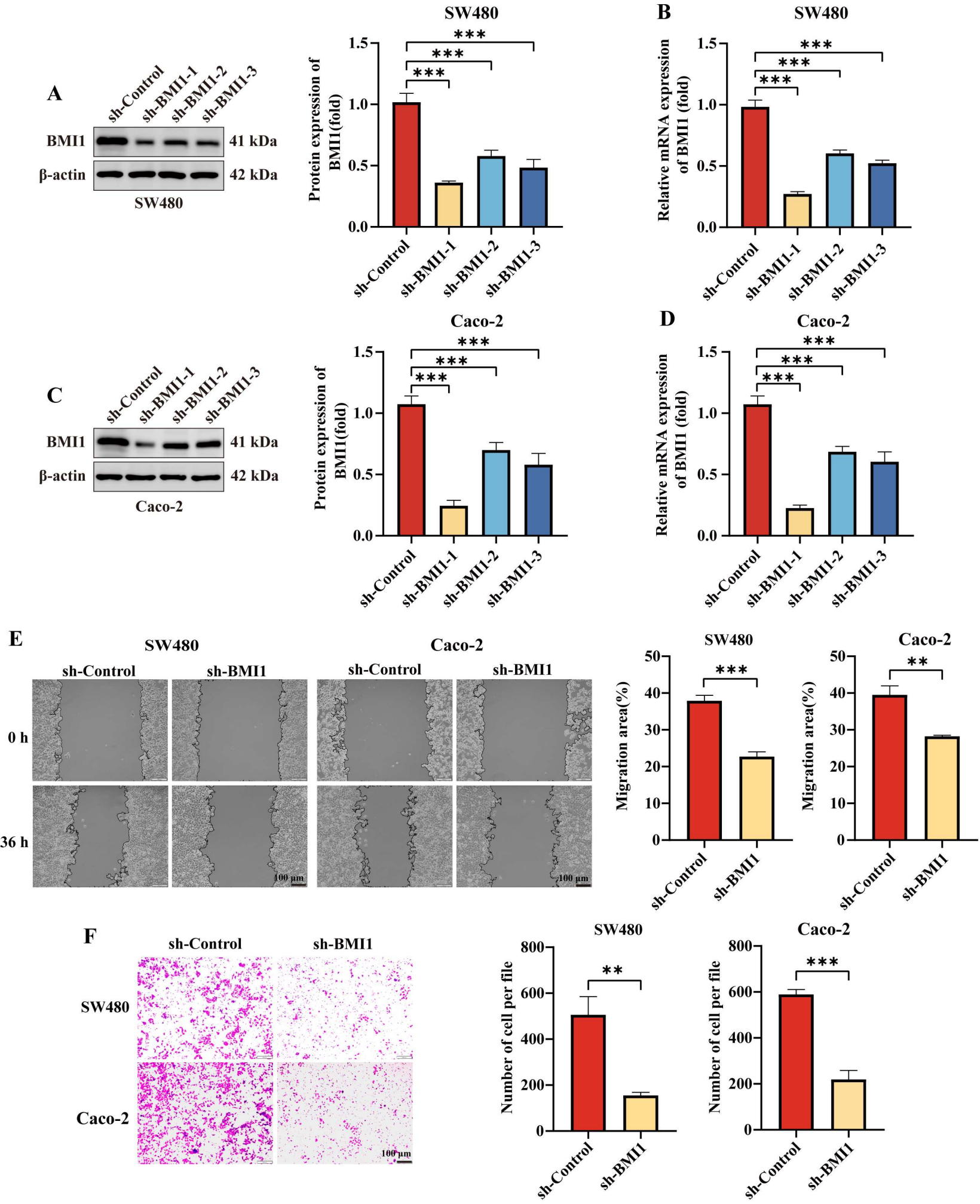
Figure. 8 Resveratrol Inhibits CRC Progression by Enhancing Cell Adhesion.

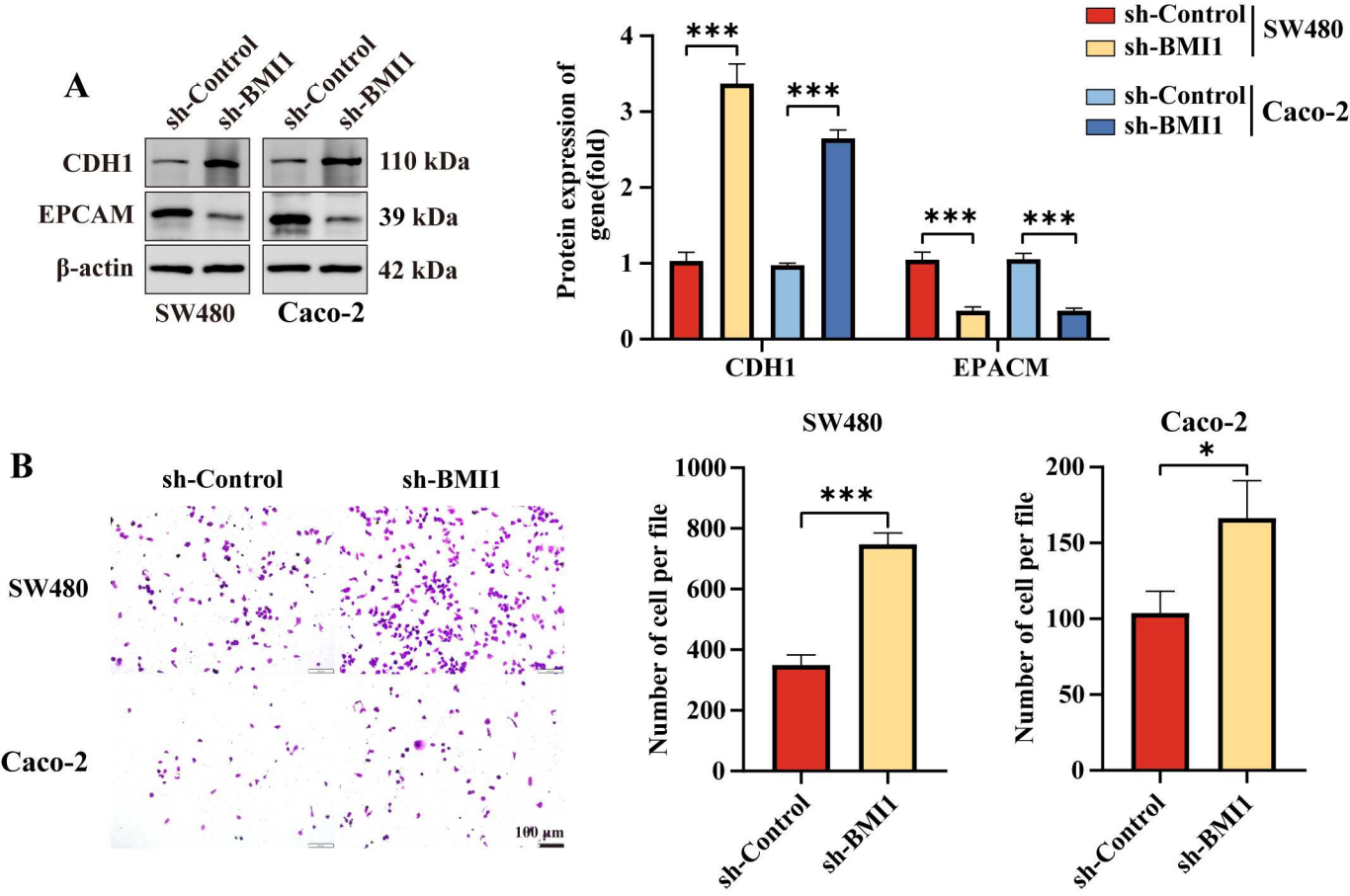
A. After treating CRC cells with Cetuximab alone (30 nM) or in combination with Resveratrol, WB analysis was performed to detect the expression levels of cell adhesion-related proteins. The WB signals were quantified, normalized to β-actin, and presented as a histogram. B. Cell adhesion assays were conducted to evaluate the effect of Cetuximab alone or in combination with Resveratrol on the adhesion ability of CRC cells. The results of the cell adhesion experiments were quantitatively analyzed. Scale bar: 100 μm. C. Typical picture of subcutaneous graftoma in nude mice. D. Tumor growth curves in each group of nude mice. E. Tumor weight statistics in each group of nude mice. F. IHC analysis of expression levels of BMI1, Ki-67, EPCAM, and CDH2 in subcutaneous graftoma tissues in nude mice. Scale bar: 100 μm. *** represents $p< 0.001$.

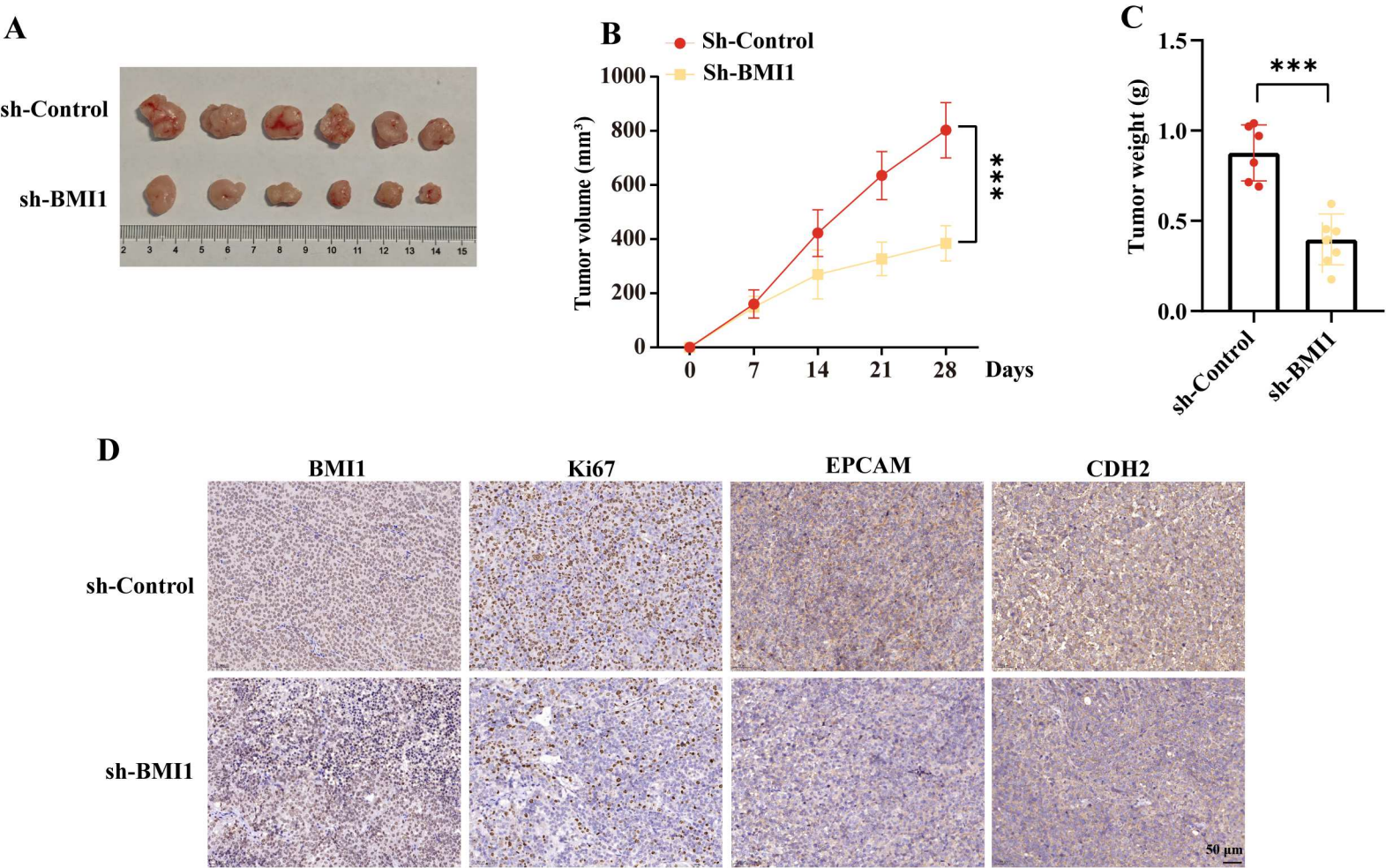
Figure. 9 Resveratrol Synergizes with Cetuximab to Inhibit CRC Progression.

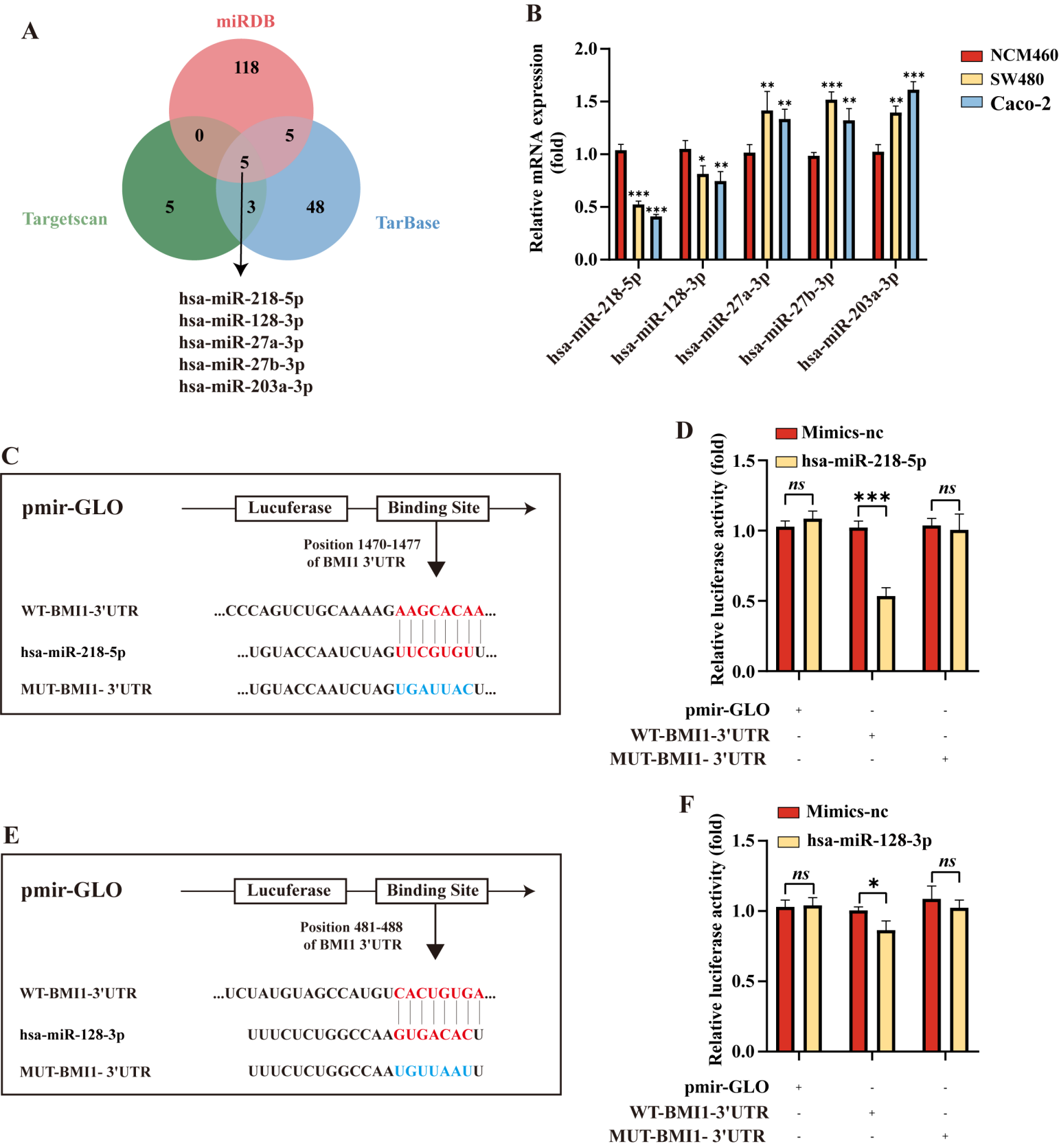
A. After treating CRC cells with Cetuximab alone (30 nM) or in combination with Resveratrol, WB analysis was performed to detect the expression levels of cell adhesion-related proteins. The WB signals were quantified, normalized to β-actin, and presented as a histogram. B. Cell adhesion assays were conducted to evaluate the effect of Cetuximab alone or in combination with Resveratrol on the adhesion ability of CRC cells. The results of the cell adhesion experiments were quantitatively analyzed. Scale bar: 100 μm. C. Representative images of subcutaneous xenograft tumors in nude mice. D. Growth curves of subcutaneous xenograft tumor volumes in nude mice. E. Statistical analysis of subcutaneous xenograft tumor weights. F. IHC analysis of the expression levels of related proteins in subcutaneous xenograft tumor tissues of nude mice from each group. ** represents $p< 0.01$, *** represents $p< 0.001$.

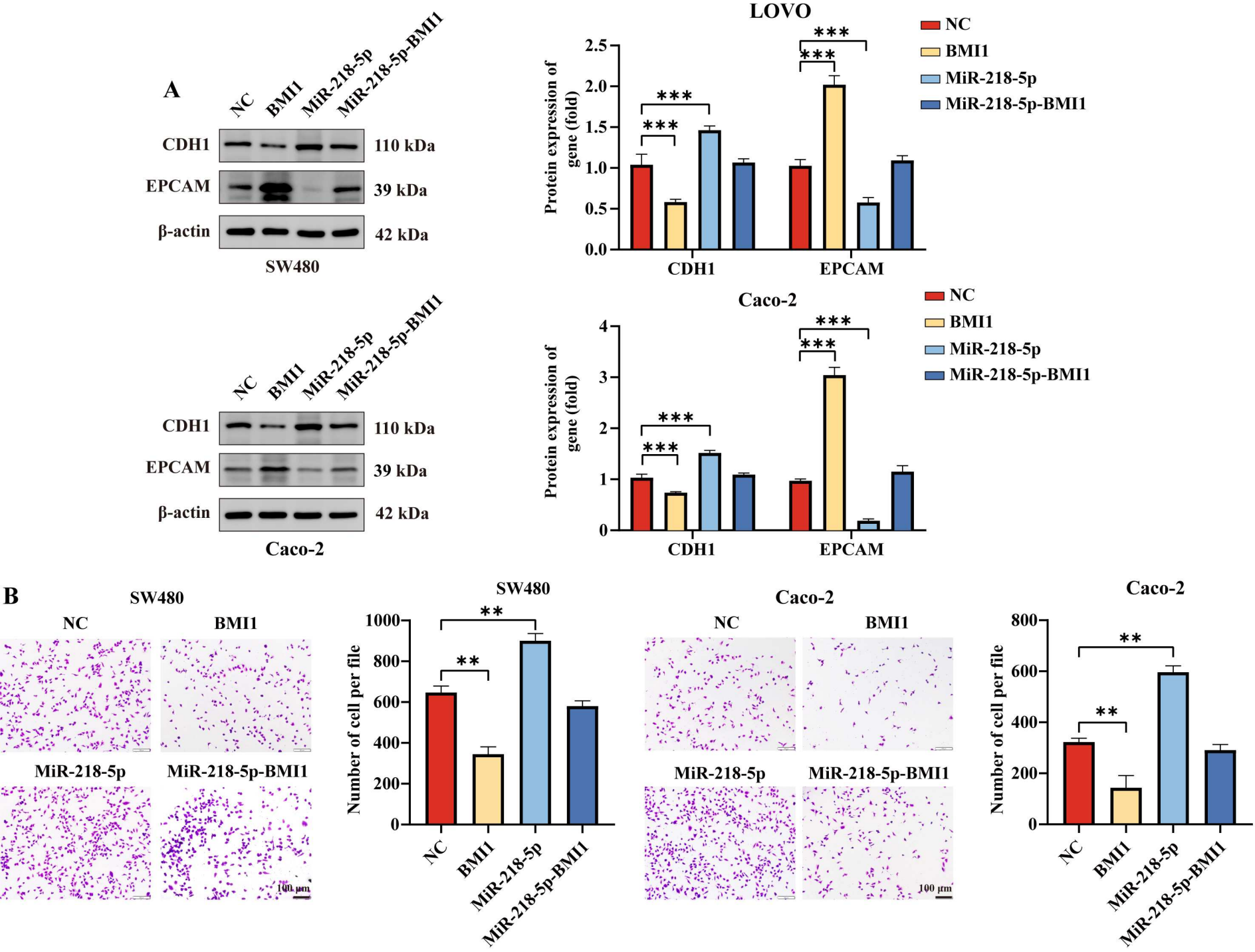

A
Patient 1
Patient 2
Patient 3
Normal
Tumor
50 μm
IHC Score
***
Normal (n=20)
Tumor (n=20)
B
1 2 3 4
N T N T N T N T
BMI1
β-actin
41 kDa
42 kDa
5 6 7 8
Protein expression of BMI1(fold)
Normal
Tumor
C
Relative mRNA expression of BMI1 (fold)
**
Normal (n=20)
Tumor (n=20)
D
NCM460
SW480
LOVO
E


A
sh-Control
sh-BMI1-1
sh-BMI1-2
sh-BMI1-3
BMI1
41 kDa
β-actin
42 kDa
SW480
SW480
Protein expression of BMI1(fold)
***
B
SW480
Relative mRNA expression of BMI1 (fold)
C
Caco-2
D
Caco-2
E
SW480
Caco-2
sh-Control
sh-BMI1
0 h
36 h
100 μm
Migration area(%)
**
F
Number of cell per file


A
sh-Control
sh-BMI1
sh-Control
sh-BMI1
CDH1
EPCAM
β-actin
110 kDa
39 kDa
42 kDa
SW480
Caco-2
sh-Control
sh-BMI1
SW480
sh-Control
sh-BMI1
Caco-2
Protein expression of gene(fold)
***
***
***
***
CDH1
EPACM
B
sh-Control
sh-BMI1
SW480
Caco-2
100 μm
SW480
Number of cell per file
***
sh-Control
sh-BMI1
Caco-2
Number of cell per file
*
sh-Control
sh-BMI1

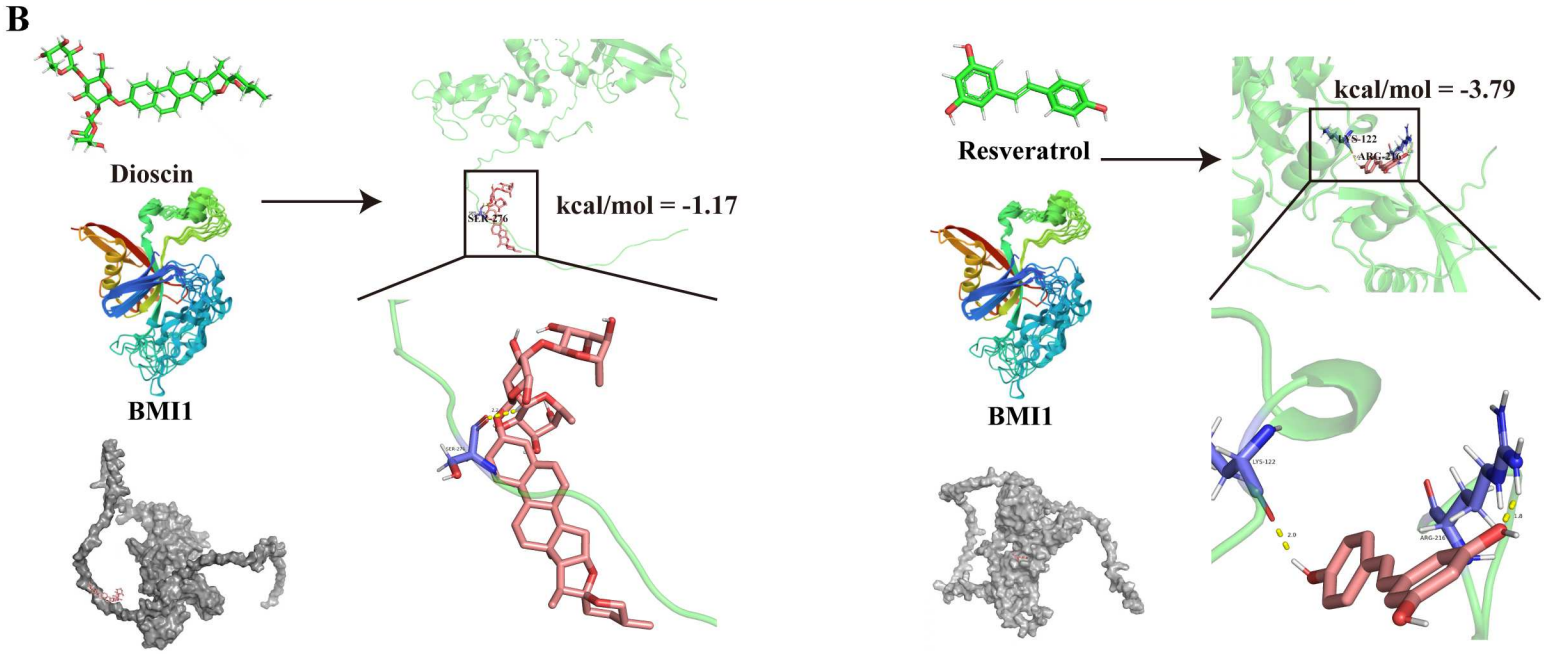

A
sh-Control
sh-BMI1
B
Sh-Control
Sh-BMI1
Tumor volume (mm³)
1000
800
600
400
200
0
***
0
7
14
21
28
Days
C
Tumor weight (g)
1.5
1.0
0.5
0.0
***
sh-Control
sh-BMI1
D
BMI1
Ki67
EPCAM
CDH2
sh-Control
sh-BMI1
50 μm

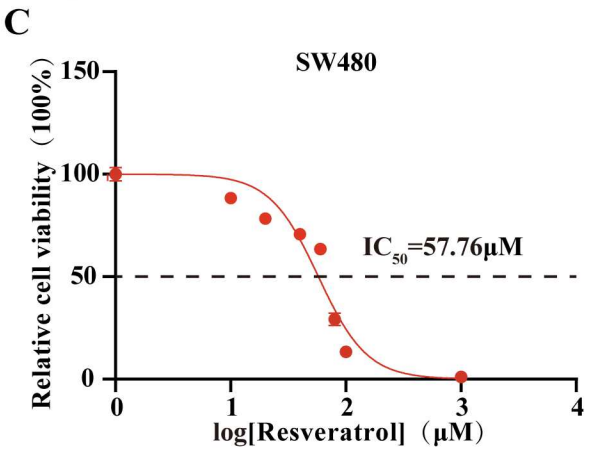

A
miRDB
118
0
5
5
5
3
48
Targetscan
TarBase
hsa-miR-218-5p
hsa-miR-128-3p
hsa-miR-27a-3p
hsa-miR-27b-3p
hsa-miR-203a-3p
B
Relative mRNA expression (fold)
NCM460
SW480
Caco-2
hsa-miR-218-5p
hsa-miR-128-3p
hsa-miR-27a-3p
hsa-miR-27b-3p
hsa-miR-203a-3p
C
pmir-GLO
Lucuferase
Binding Site
Position 1470-1477 of BMI1 3'UTR
WT-BMI1-3'UTR ...CCCAGUCUGCAAAAGAAGCACAA...
hsa-miR-218-5p ...UGUACCAAUCUAGUUCGUGUU...
MUT-BMI1- 3'UTR ...UGUACCAAUCUAGUGAUUACU...
D
Mimics-nc
hsa-miR-218-5p
Relative luciferase activity (fold)
ns
***
ns
pmir-GLO + - -
WT-BMI1-3'UTR - + -
MUT-BMI1- 3'UTR - - +
E
pmir-GLO
Lucuferase
Binding Site
Position 481-488 of BMI1 3'UTR
WT-BMI1-3'UTR ...UCUAUGUAGCCAUGUCACUGUGA...
hsa-miR-128-3p UUUCUCUGGCCAAGUGACACU
MUT-BMI1- 3'UTR UUUCUCUGGCCAAUGUUAAUU
F
Mimics-nc
hsa-miR-128-3p
Relative luciferase activity (fold)
ns
*
ns
pmir-GLO + - -
WT-BMI1-3'UTR - + -
MUT-BMI1- 3'UTR - - +

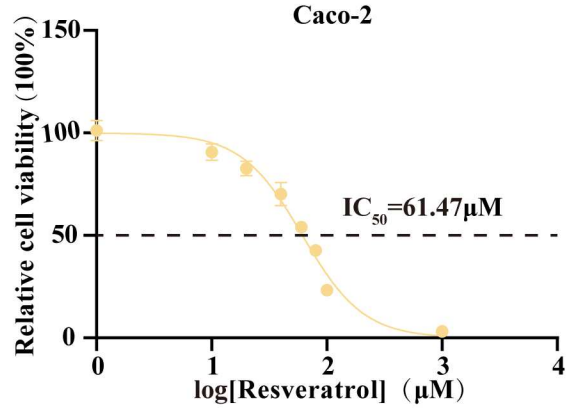

A
NC
BMI1
MiR-218-5p
MiR-218-5p-BMI1
CDH1
EPCAM
β-actin
110 kDa
39 kDa
42 kDa
SW480
Caco-2
LOVO
Protein expression of gene (fold)
***
**
B
100 μm
Number of cell per file

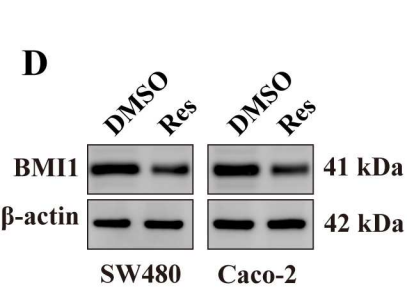
A

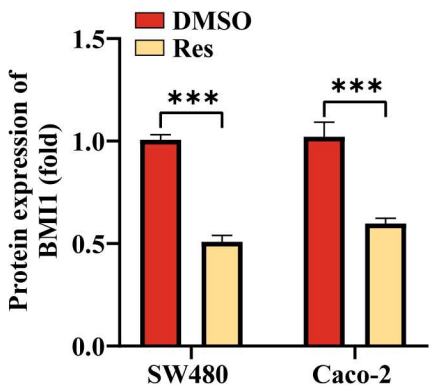
Drug Name	Binding energy (kcal/mol)	Site-specific amino acid residues	Hydrogen bond length
Dioscin	-1.17	SER-276	2.2
Resveratrol	-3.79	LYS-122	2.0
		ARG-216	1.8

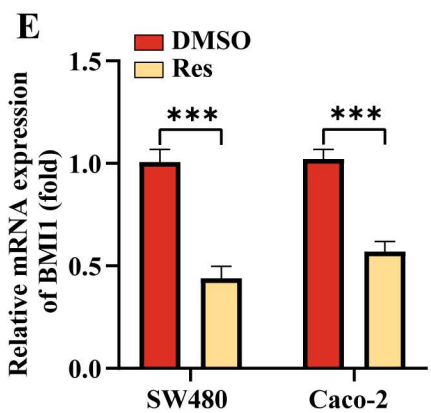


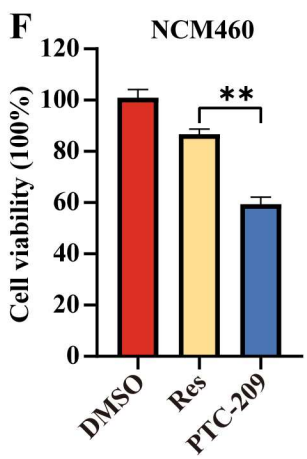


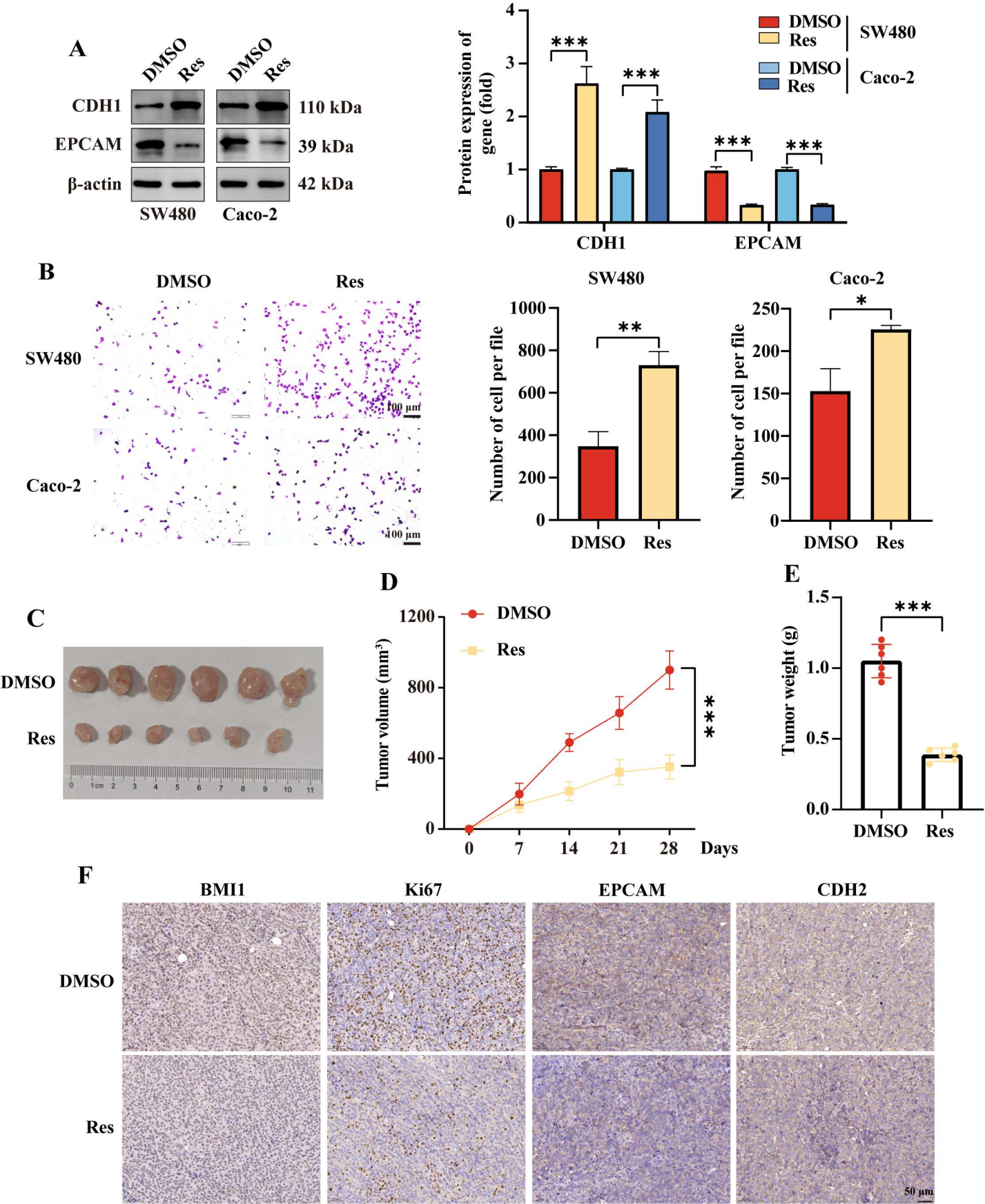


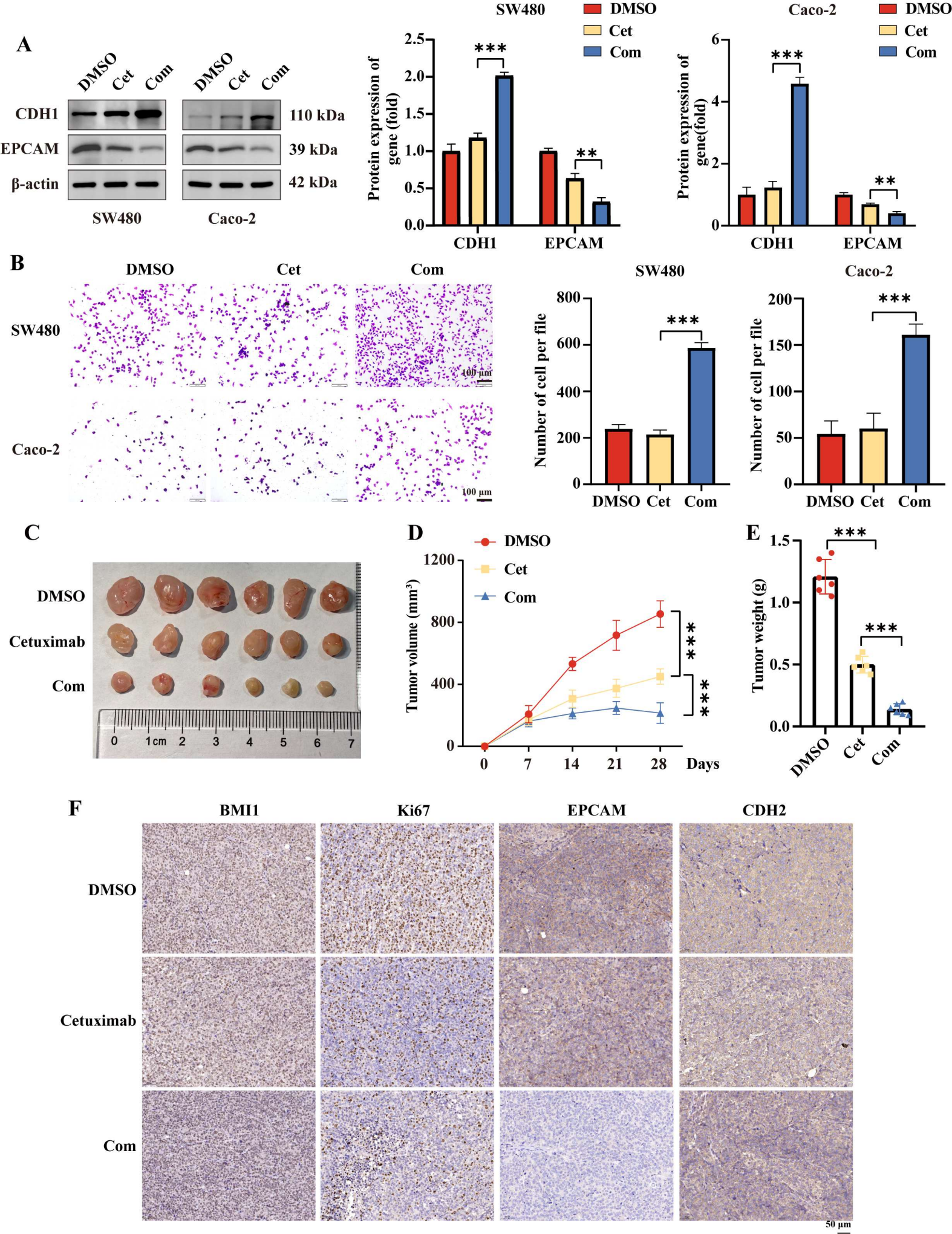









A
DMSO
Res
DMSO
Res
CDH1
EPCAM
β-actin
110 kDa
39 kDa
42 kDa
SW480
Caco-2
Protein expression of gene (fold)
DMSO
Res
SW480
DMSO
Res
Caco-2
***
***
***
***
CDH1
EPCAM
B
DMSO
Res
SW480
Caco-2
100 μm
100 μm
SW480
Caco-2
Number of cell per file
**
*
DMSO
Res
C
DMSO
Res
D
DMSO
Res
Tumor volume (mm³)
***
Days
E
Tumor weight (g)
***
DMSO
Res
F
BMI1
Ki67
EPCAM
CDH2
DMSO
Res
50 μm


A
DMSO
Cet
Com
CDH1
EPCAM
β-actin
110 kDa
39 kDa
42 kDa
SW480
Caco-2
SW480
DMSO
Cet
Com
Protein expression of gene (fold)
***
**
CDH1
EPCAM
Caco-2
DMSO
Cet
Com
Protein expression of gene(fold)
***
**
CDH1
EPCAM
B
DMSO
Cet
Com
SW480
Caco-2
100 μm
100 μm
SW480
Number of cell per file
***
DMSO
Cet
Com
Caco-2
Number of cell per file
***
DMSO
Cet
Com
C
DMSO
Cetuximab
Com
0
1cm
2
3
4
5
6
7
D
DMSO
Cet
Com
Tumor volume (mm³)
***
***
Days
E
Tumor weight (g)
***
***
DMSO
Cet
Com
F
BMI1
Ki67
EPCAM
CDH2
DMSO
Cetuximab
Com
50 μm

Supplementary Table

Table 1. Primer information required for RT-qPCR process.

Primer name	Primer sequence (5′–3′)
BMI1-Forward	GCTGCCAATBMI1CTAATGAA
BMI1-Reverse	TGCTGGGCATCGTAAGTATCTT
β-Actin-Forward	CACCATTGGCAATGAGCGGTTC
β-Actin -Reverse	AGGTCTTTGCGGATGTCCACGT
MiR-218-5p-Forward	CGAGTGCATTTGTGCTTGATCTA
MiR-218-5p-Reverse	TAATGGTCGAACGCCTAACGTC
U6-Forward	CTCGCTTCGGCAGCACA
U6-Reverse	AACGCTTCACGAATTTGCGT

Supplementary Files

This is a list of supplementary files associated with this preprint. Click to download.

- Supplementarymaterials.docx